Electronic structure, phase stability, and magnetic properties of $La_{1-x}Sr_xCoO_3$ from first-principles full-potential calculations

P. Ravindran*
Department of Chemistry, University of Oslo, Box 1033, Blindern, N-0315 Oslo, Norway

P. A. Korzhavyi
Condensed Matter Theory Group, Department of Physics, Uppsala University, Box 530, 75121 Uppsala, Sweden

H. Fjellvåg
Department of Chemistry, University of Oslo, Box 1033, Blindern, N-0315 Oslo, Norway

A. Kjekshus
Department of Chemistry, University of Oslo, Box 1033, Blindern, N-0315 Oslo, Norway
(Received 23 June 1999)

In order to understand the role of hole doping on electronic structure, phase stability and magnetic properties of $LaCoO_3$ generalized-gradient-corrected, relativistic first-principles full-potential density functional calculations have been performed for $La_{1-x}Sr_xCoO_3$ as a function of x, using the supercell approach as well as the virtual crystal approximation (VCA). It has been shown that the rhombohedral distortion is stabilizing the nonmagnetic (i.e., diamagnetic or paramagnetic) ground state in $LaCoO_3$. Spin-polarized calculation on the hypothetical cubic perovskite phase of $LaCoO_3$ shows that the ferromagnetic phase is lower in energy than the corresponding nonmagnetic phase. The analysis of the electronic structures show that a Peierls-Jahn-Teller-like instability arises in the ferromagnetic cubic phase and leads to the rhombohedral distortion in $LaCoO_3$. The calculated magnetic moment for $La_{1-x}Sr_xCoO_3$ as a function of Sr substitution is found to be in very good agreement with recent neutron scattering measurements. We have successfully explained the hole-doping induced, nonmagnetic-to-ferromagnetic transition as well as the rhombohedral-to-cubic structural transition as a function of Sr substitution in $La_{1-x}Sr_xCoO_3$. Due to the failure of the density functional theory to predict the semiconducting nature of $LaCoO_3$, we are unable to explain the experimentally observed semiconductor-to-metal transition in $LaCoO_3$ by Sr substitution. The origin of the ferromagnetism in $La_{1-x}Sr_xCoO_3$ has been explained through itinerant-band ferromagnetism. [S0163-1829(99)14047-5]

I. INTRODUCTION

In recent years the number of experimental as well as theoretical studies on the perovskite $3d$ transition metal oxides of ABO_3 type have increased by the discovery of high-T_c superconductivity in perovskite cuprates[1] and the observation of a colossal negative magnetoresistance near room temperature in perovskitelike La-Ba-Mn-O films.[2] Depending on the transition metal ion, perovskites exhibit either localized or collective behavior of the d electrons. Also depending upon the valence of the A cation, the valence of the transition metal ion changes and this leads to unusual magnetic and electronic properties.

Lanthanum cobalt oxide ($LaCoO_3$) has attracted much attention in the past because it shows fascinating changes in the electronic and magnetic properties as a function of temperature and/or divalent substitution. It is a charge-transfer-type insulator in which the charge gap is formed between the occupied O $2p$ and the unoccupied Co $3d$ e_g band.[3] However, studies by soft-x-ray absorption (XAS) (Ref. 4) and electron spectroscopies,[5] have revealed that $LaCoO_3$ is in the highly mixed character region between Mott-Hubbard and charge-transfer insulators. The crystal field splitting Δ_{cf} is almost equal to the exchange energy Δ_{ex} and this causes spin-state transition[4,6–10] as well as electrical and magnetic phase transformations[6,7,11–14] in $LaCoO_3$ as a function of temperature and/or hole doping. One of the most interesting properties of this oxide is its unusual temperature-dependent magnetic susceptibility. Co^{3+} ions take nominally the $3d^6$ configuration and will have nonmagnetic (i.e., diamagnetic or paramagnetic) low spin (LS) state ($t_{2g}^6 e_g^0$; $S=0$) due to a crystal field splitting ($10Dq$) slightly larger than the Hund's rule coupling.[11] But, $LaCoO_3$ exhibits an abrupt increase of magnetic susceptibility around 50–100 K which thereafter decreases following the Curie-Weiss law.[7,15] This anomalous behavior has been interpreted as a transition from the LS, nonmagnetic ($S=0$) state to thermally excited high-spin (HS) magnetic ($t_{2g}^4 e_g^2$; $S=2$) state with a spin-gap energy of $0.01-0.08$ eV.[4–9,11,15–20] With a further increase of temperature, the electrical conduction of $LaCoO_3$ shows a crossover around 500 K from thermally activated semiconduction to metallic conduction ($\rho \approx 1.10^{-3}$ Ω cm).[16] Recent neutron-scattering measurements show that this nonmetal-to-metal crossover behavior has no magnetic origin.[14]

The more recent optical conductivity measurements indicate that the high temperature metallic state in $LaCoO_3$ has an electronic structure very similar to that of a doping-induced metallic state.[21] Raccah and Goodenough[19] found

that the semiconductor-to-metal transition takes place around $x=0.3$ in $La_{1-x}Sr_xCoO_3$ without any abrupt change in the resistivity. The transport measurements by Bhide *et al.*[22] show that the semiconductor-to-metal transition takes place around $x\approx0.125$ and spectroscopic measurements indicate that the transition is at $x\approx0.2$.[5] Recent electrical conductivity measurements[23] show that the transition takes place in $La_{1-x}Sr_xCoO_3$ at $x\approx0.25$ around room temperature. Moreover, the rhombohedral distortion decreases with increasing Sr concentration and the rhombohedral-to-cubic structural transition takes place around the composition $La_{0.5}Sr_{0.5}CoO_3$. Furthermore, $La_{1-x}Sr_xCoO_3$ has also been extensively investigated to understand the role of hole doping on the spin-state transition and magnetic properties of $LaCoO_3$.[18,19,22,24–26] Since the hole-doping-induced electronic structure change is equivalent to temperature-induced change, it is interesting to study the electronic structure of $LaCoO_3$ as a function of Sr doping to understand the microscopic origin of the temperature-induced anomalous behavior. This is one of the motivations for the present investigation.

In the past the magnetism in $La_{1-x}Sr_xCoO_3$ has been explained by Anderson's[27] theory of superexchange interaction and the Zener's[28] double-exchange-interaction theory. From the magnetic measurements on $La_{1-x}Sr_xCoO_3$ by Jonker and van Santen[24] ($0\leqslant x\leqslant0.5$) and by Taguchi *et al.*[25] ($0.5\leqslant x\leqslant1$) the magnetic properties of Sr substituted $LaCoO_3$ has been explained through superexchange interaction between cobalt ions via oxygen. To explain the composition dependent magnetic properties of $La_{1-x}Sr_xCoO_3$, Goodenough[29] assumed that the covalent mixing between the transition metal $3d$ orbitals and the oxygen $2p$ orbitals may enhance the superexchange interaction and break down the conditions for localized d electrons. Bhide *et al.*[22] measured the temperature dependence of Mössbauer spectra for the ferromagnetic region of $La_{1-x}Sr_xCoO_3$ ($0\leqslant x\leqslant0.5$) and concluded that the $3d$ holes created by the Sr-ion substitution are itinerant both above and below Curie temperature (T_c) and all the experimental data are explained on the basis of itinerant-electron ferromagnetism. Recently Golovanov *et al.*[30] made dc resistivity, magnetoresistance and magnetic susceptibility studies for $La_{1-x}Sr_xCoO_3$ ($0.05\leqslant x\leqslant0.25$) as a function of temperature as well as magnetic field and the results were interpreted in terms of Zener's[28] double-exchange mechanism. The conventional itinerant-electron ferromagnets such as Fe, Co, or Ni have charge carriers which are mainly of s character while the magnetism arises from the d electrons. However, in the itinerant-electron ferromagnetic oxides, the d electrons have to possess simultaneously charge as well as spin character.[31] Hence the understanding of the origin of the itinerant electron behavior and ferromagnetism in $La_{1-x}Sr_xCoO_3$ would be of fundamental importance.

From the resonance photoemission spectra combined with configuration-interaction cluster model calculations Saitoh *et al.*[32] concluded that ferromagnetic phase of $La_{1-x}Sr_xCoO_3$ are in the intermediate spin (IS) state ($S=1$). From magnetic measurements, Taguchi *et al.*[25] propose that Co^{3+} are in the LS state and Co^{4+} are in the HS state in $La_{1-x}Sr_xCoO_3$ ($0.5\leqslant x\leqslant1$). The time-averaged electron configuration of cobalt seen in the Mössbauer spectra[22] and by electron-transport properties[19] show that the d electrons in $La_{1-x}Sr_xCoO_3$ become itinerant when $x>0.125$. Although so far several explanations are given regarding the magnetic interactions in $La_{1-x}Sr_xCoO_3$, no systematic theoretical attempt has yet been made to understand microscopically the origin of the magnetic properties of $LaCoO_3$ by hole doping and this also motivated the present study.

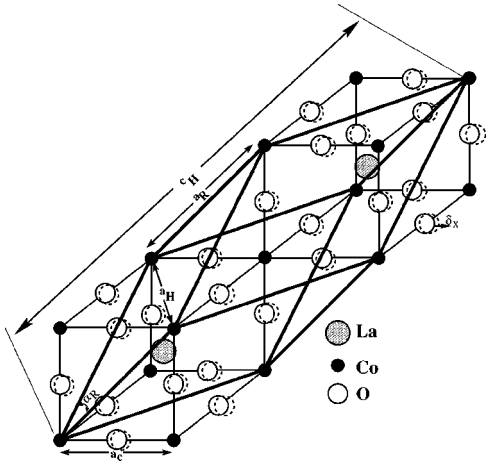

FIG. 1. Crystal structure of rhombohedral $LaCoO_3$ in relation to the cubic perovskite structure. a_R and α_R refer to the rhombohedral setting of the unit cell and a_H and c_H to the hexagonal setting. The oxygen atoms in the rhombohedral arrangement are displaced with respect to the cubic structure by δx and the displacement is indicated by dotted circles.

The studies on these compounds are not only of fundamental interest, but also have technological significance. $La_{1-x}Sr_xCoO_3$ ($x=0-0.6$) is a well known ionic conductor that has large diffusion coefficients for O^{2-} as compared with other metal oxides.[33,34] As the strontium doped lanthanum cobaltites also possess high electrical conductivity, these are promising cathod materials for use in solid oxide fuel cells[35,36] and for oxygen permeable membranes.[37] These compounds have furthermore high catalytic activity for the oxidation of CO, hydrocarbons, and alcohols[38] and the elimination of NO.[39] Fairly large magnetoresistance has recently been observed for $La_{1-x}A_xCoO_3$ (A=Ca, Sr, or Ba) in bulk[40] as well as in thin films.[41]

The rest of this paper is organized in the following way. In Sec. II we give details about the crystal structure of $La_{1-x}Sr_xCoO_3$. In Sec. III, we explain the computational method used in the present calculations. In Sec. IV, we discuss the electronic structure and magnetic properties of $LaCoO_3$ as a function of Sr substitution. The calculated results are furthermore compared with the available experimental results. Finally in Sec. V the findings in the present study are summarized.

II. STRUCTURAL ASPECTS

$LaCoO_3$ has a rhombohedrally distorted pseudo-cubic perovskite structure. The space group is $R\bar{3}c$ and each unit cell contains two formula units. With respect to the cubic structure, the O atoms are twisted around the crystallographic [111] making the symmetry trigonal D_{3d}^6. Figure 1 shows the unit cell of $LaCoO_3$; indicating both the rhombohedral and hexagonal axes and the cubic subcell. The CoO_6

octahedron is slightly compressed along the hexagonal c axis. The displacements of the oxygen atoms with respect to the ideal cubic structure are represented by the dotted circles and specified with the distortion parameter δx in Fig. 1. When the (Goldschmidt) tolerance factor $t = d_{A\text{-}O}/\sqrt{2}d_{B\text{-}O}$ is less than unity in the ABO_3-type perovskites, a cooperative rotation of the corner-shared BO_6 octahedra about [111] reduces the symmetry from cubic to rhombohedral. The regular octahedra are topologically able to rotate without distortion around their threefold axes. The magnitude of the rotation can be evaluated from either the angle α of the rhombohedral unit cell shown in Fig. 1 or from the axial ratio c_H/a_H of the hexagonal cell. For the ideal (cubic) perovskite configuration $c_H/a_H = \sqrt{6}$, $\alpha = 60°$, and the bond angle B-O-B is 180°. As a result of the rotation (tilting), the Co-O-Co bond bends[42] and the angle (163.2°) deviates from the ideal perovskite value.

$La_{1-x}Sr_xCoO_3$ stabilizes in the rhombohedral structure with space group $R\bar{3}c$ in the range $0 \leqslant x \leqslant 0.5$ and transforms to a cubic phase with the space group $Pm\bar{3}m$ at higher substitution levels. The rhombohedral distortion decreases with increase of x. A similar variation results from thermal expansion for the parent compound $LaCoO_3$. In $LaCoO_3$, La atoms are in $2a$ $(\frac{1}{4},\frac{1}{4},\frac{1}{4})$, Co atoms are in $2b$ (0 0 0), and O atoms in $6e$ $(\frac{1}{4}+\delta x, \frac{1}{4}-\delta x, \frac{3}{4})$ position. In $La_{1-x}Sr_xCoO_3$, δx decreases from 0.052 for $x=0$ to 0.014 for $x=0.5$. The rhombohedral angle also decreases with increasing x; for $x=0$ it is 60.79° and is reduced to 60.27° for $x=0.5$. The cubic phase may be viewed as a special case of the rhombohedral structure with $\delta x = 0$ and $\alpha = 60°$ as shown in Fig. 1. As the ionic radius of the Sr ion is larger than that of the La ion, the unit cell effectively expands when La is replaced by Sr in $La_{1-x}Sr_xCoO_3$. Thereby the tolerance factor will increase and this leads to the rhombohedral-to-cubic structural transition.

$SrCoO_3$ is a ferromagnet with a Curie temperature of 222 K and stabilizes in the cubic perovskite structure. The Co ions are octahedrally coordinated with oxygen ions, while the Sr ions are twelvefold coordinated with oxygens along $\langle 110 \rangle$. High Sr^{2+} substitution levels tend to induce oxygen deficiency. For $SrCoO_3$ without oxygen deficiency the lattice parameter is determined to be $a = 3.836$ Å from extrapolation of the experimental[25] relation between oxygen content and lattice parameter. The structural data for the rhombohedral structure of $La_{1-x}Sr_xCoO_3$ $(x = 0-0.5)$ are taken from a recent neutron diffraction study,[43] whereas, data for the cubic composition range $(0.5 < x \leqslant 1)$ are taken from Ref. 25. The structural parameters for the cubic and rhombohedral phases of $La_{1-x}Sr_xCoO_3$ used in the present calculations are given in Table I.

TABLE I. The structural parameters for cubic and rhombohedral phases of $La_{1-x}Sr_xCoO_3$ used in the present calculations. a_R and a_C represent the lattice constants for the rhombohedral and cubic phase respectively (in Å) and α represent the rhombohedral angle (in degrees). The oxygen parameters for the 6(e) position (x,y,z) for the rhombohedral lattice are also given.

Sr content (x)	a_R	α	x	y	z	a_C
0	5.37	60.79	0.3021	0.1978	0.75	3.805
0.1	5.32	60.49	0.292	0.208	0.75	
0.2	5.36	60.45	0.289	0.211	0.75	
0.25	5.34	60.46	0.2835	0.2165	0.75	3.789
0.3	5.32	60.47	0.278	0.222	0.75	
0.4	5.35	60.30	0.274	0.226	0.75	
0.5	5.35	60.27	0.264	0.236	0.75	3.791
0.75	5.41	60.00	0.25	0.25	0.75	3.827
1.0	5.424	60.00	0.25	0.25	0.75	3.836

III. COMPUTATIONAL DETAILS

The full-potential LMTO calculations[44] presented in this paper are all electron and no shape approximation to the charge density or potential has been used. The base geometry in this computational method consists of a muffin-tin part and an interstitial part. The basis set is comprised of augmented linear muffin-tin orbitals.[45] Inside the muffin-tin spheres the basis functions, charge density, and potential are expanded in symmetry adapted spherical harmonic functions together with a radial function and a Fourier series in the interstitial. In the present calculations the spherical-harmonic expansion of the charge density, potential, and basis functions were carried out up to $l_{\max} = 6$. The tails of the basis functions outside their parent spheres are linear combinations of Hankel or Neumann functions depending on the sign of the kinetic energy of the basis function in the interstitial region. For the core charge density, the Dirac equation is solved self-consistently, i.e., no frozen core approximation is used. The calculations are based on the generalized-gradient-corrected density functional theory as proposed by Perdew and Wang.[46]

In the calculation of the radial functions inside the muffin-tin spheres, all scalar-relativistic terms are included, with the small component vanishing at the sphere boundary. The spin-orbit (SO) term is included directly in the Hamiltonian matrix elements for the part inside the muffin-tin spheres, thus doubling the size of the secular matrix for a spin-polarized calculation. Moreover, the present calculations make use of a so-called multibasis, to ensure a well converged wave function. This means that we use different Hankel or Neuman functions each attaching to its own radial function. We thus have two $6s$, two $5p$, two $6p$, two $5d$, and two $4f$ orbitals for La, two $4s$, two $5p$, and three $3d$ orbitals for Co, two $2s$, three $2p$, and two $3d$ orbitals for O, two $5s$, two $4p$, two $5p$, and two $4d$ for Sr in our expansion of the wave function. In the method used here, bases corresponding to multiple principal quantum numbers are contained within a single, fully hybridizing basis set. The direction of the moment is chosen to be in (001) direction. The calculations were performed for the cubic perovskite structure as well as the rhombohedral $R\bar{3}c$ structure. The **k**-space integration was performed using the special point method with 84 **k** points in the irreducible part of the first Brillouin zone for the cubic perovskite structure and the same density of **k** points were used for the rhombohedral structure in the supercell as well as the virtual-crystal-approximation (VCA) calculations. All the calculations were done using the experimental structural parameters mentioned in Sec. II for both the nonmagnetic as well as the spin-polarized case. Our VCA calculation takes into account the experimentally reported[43]

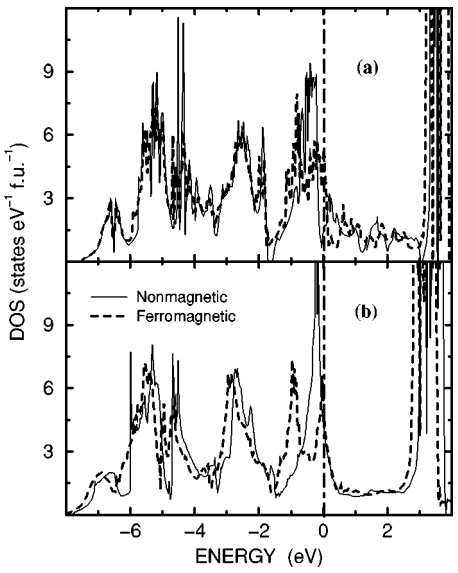

FIG. 2. Calculated total density of states (DOS) for $LaCoO_3$ in the ferromagnetic and nonmagnetic phases of (a) rhombohedral and (b) cubic structures.

structural parameter changes as a function of Sr substitution. Hence, the VCA calculations have taken into account the hybridization effect properly. In this approximation the true atom in the phase is replaced by an ''average'' atom which is interpolated linearly in charge between the corresponding pure atoms. So for the VCA calculations we have not properly taken into account the charge transfer effect, although the band-filling effects are accounted properly. The chosen approximation has an advantage due to its simplicity and hence we can be able to study small concentrations of Sr in $LaCoO_3$. However, for 25, 50, and 75 % Sr substitution we have made explicit supercell calculations for the cubic as well as the rhombohedral structure. Using the self-consistent potentials obtained from our supercell calculations, the density of states (DOS) were calculated using the linear tetrahedron technique.

IV. RESULTS AND DISCUSSION

A. Electronic structure

For a compound with an octahedrally coordinated d^6 ion, the low-spin state ($t_{2g}^6 e_g^0$) is more stable than the high-spin state ($t_{2g}^4 e_g^2$) when $10Dq \geqslant 2J$, $10Dq$ being the cubic crystal field and J the intra-atomic exchange interaction.[47] The electronic structure of perovskite-type transition-metal oxides are described by the three crucial energy parameters, the bandwidth W, the Coulomb repulsive energy U, and the strength (Dq) of the ligand field. In the cubic perovskites, the octahedral ligand field produced by the O atoms surrounding each Co atom split the tenfold degenerate d levels of Co into sixfold t_{2g} and fourfold e_g levels. The electronic structure of these materials can be understood by the schematic energy diagram proposed by Goodenough.[48] In such a picture, the e_g orbitals of the Co atom form σ bonds with O $2p$ orbitals whereas t_{2g} orbitals form weaker π bonds with O $2p$ orbitals. As mentioned by Arima,[49] the hybridization between Co $3d$ and O $2p$ is important to explain the electronic structure of $LaCoO_3$. Because of the strong covalent hybridization of

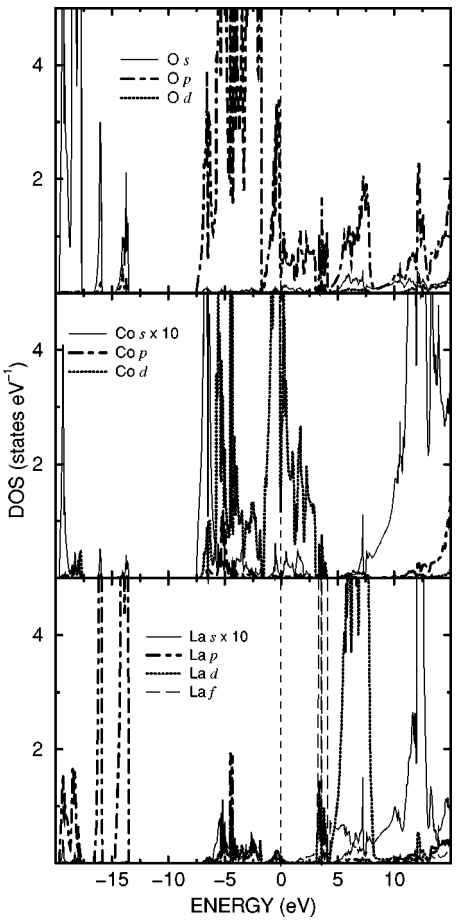

FIG. 3. Angular-momentum-site-projected DOS for $LaCoO_3$ in the nonmagnetic rhombohedral structure. Note that DOS for La s and Co s have been multiplied by a factor of 10.

Co $3d$ with the neighboring O $2p$ states, the calculated DOS curves shown in Fig. 2 show broad features. In general a large U tends to split bands into spin-up and spin-down bands. Because of the extended electronic states the Coulomb repulsive energy would be small compared with the band width, and hence one can expect a nonmagnetic ground state in $LaCoO_3$. Consistent with the above viewpoint, experimental observations as well as our calculations show that the nonmagnetic state is the ground state for $LaCoO_3$.

The angular momentum and site projected DOS for $LaCoO_3$ are shown in Fig. 3. From this figure it is clear that the present theory is unable to predict the semiconducting behavior of $LaCoO_3$, as there is finite density of states present at the Fermi level (E_F). In general the LDA underestimate the band gap of the materials. It is interesting to note that the optical conductivity studies[16] show a spin-gap energy of ~ 30 meV and a charge-gap of ~ 0.1 eV in this material. Further, low-temperature resistivity data[7,19,24,50] suggest a gap of about 0.2 eV whereas high-temperature resistivity indicates[12] a gap of 0.5 eV and electron-spectroscopy measurements[5,32] a conductivity gap of 0.6 eV. As the optical conductivity measurements are more reliable, the possible reasons for the failure to predict the semiconducting behavior of $LaCoO_3$ by the present theory may be the small value of the charge gap, which is within the accuracy of the present type of calculations. Further, the minimum energy gap is a spin gap indicating that $LaCoO_3$ is not

a band insulator. It should be noted that the LDA+U method, where the Co $3d$ orbitals are treated localized through describing the Coulomb intrashell interactions by the Hubbard-like term and the itinerant states are treated through averaged LDA energy and potentials, gives a bandgap of ~ 2 eV (Refs. 51,52) and the Hartree-Fock calculation gives a bandgap of 3 eV.[53] Although the present theory is unable to predict the narrow bandgap behavior in $LaCoO_3$, E_F falls on a pseudogap separating the bonding states from the antibonding states in Fig. 2. The present finding of metallic behavior is consistent with the previous theoretical studies.[54–56] It is interesting to note that LDA+U as well as HF calculations give an unphysically large bandgap in this material. Our total DOS curve for $LaCoO_3$ in the rhombohedral nonmagnetic phase in Fig. 2 show that some parts of the e_g orbitals are below the Fermi energy and mixed with the t_{2g} orbitals. However, experimental spectroscopic studies[5] indicate that a finite energy separation exists between the t_{2g} and e_g states and hence the semiconducting behavior arises. Although the non-spin-polarized calculation for $LaCoO_3$ turns out to predict metallic behavior, the density of states at the Fermi level is very low, 1.449 states eV^{-1} $f.u.^{-1}$. This probably also indicates that $LaCoO_3$ is close to semiconducting. However, the nonmagnetic nature of the ground state of $LaCoO_3$ indicates that the magnetic interactions are relatively unimportant and that the crystal field splitting is responsible for the insulating properties. Munakata *et al.*[57] suggested from analysis of the x-ray photoemisson spectrum that the top of the valence band (VB) should be assigned mainly to O $2p$. Recently, Saitoh *et al.*,[58] suggest that $LaCoO_3$ does not have a d-d or p-d gap, but a p-p gap. As the calculated DOS show a pseudogap in the vicinity of Fermi level, we can identify the nature of the band gap in this material. From Fig. 3 it is evident that the top of valence band near E_F is dominated by the Co $3d$ to O $2p$ hybridized band and the nearby bottom of the conduction band mainly consists of Co $3d$ states. This indicates that the semiconducting behavior mainly arises from the covalent interaction between Co and O within the CoO_6 octahedra.

The total DOS of $LaCoO_3$ in the nonmagnetic rhombohedral structure given in Fig. 2(a), shows that the O $2p$ and Co $3d$ states are hybridized and forms the valence band. A broad structure appears above E_F mainly originating from hybridization of the unoccupied Co e_g and O $2p$ states. Around the top of VB a sharp peak occurs which mainly arises from the Co $3d$ states. Photoemission spectra obtained with decreasing incident photon energy show[32,59] that the intensity of the peak around the top of VB decreases considerably. Since the cross section of the Co $3d$ states relative to that of the O $2p$ states becomes smaller with decreasing photon energies, this experimental fact lends support to the present finding that the features around the top of VB consist mainly of Co $3d$ states. From resonant photoemission studies, Taguchi *et al.*[25] found that the bands in VB of $LaCoO_3$ are located in a binding energy range of $0-9$ eV and comprise apparently three peaks at 1, 3, and 5 eV and a shoulder at 7 eV. Our calculated total DOS for $LaCoO_3$ in the nonmagnetic rhombohedral phase [Fig. 2(a)] gives a VB width of ~ 8 eV and shows also three prominent peaks in the VB region with energy peaks at -0.5, -2.6, and -5.2 eV. The

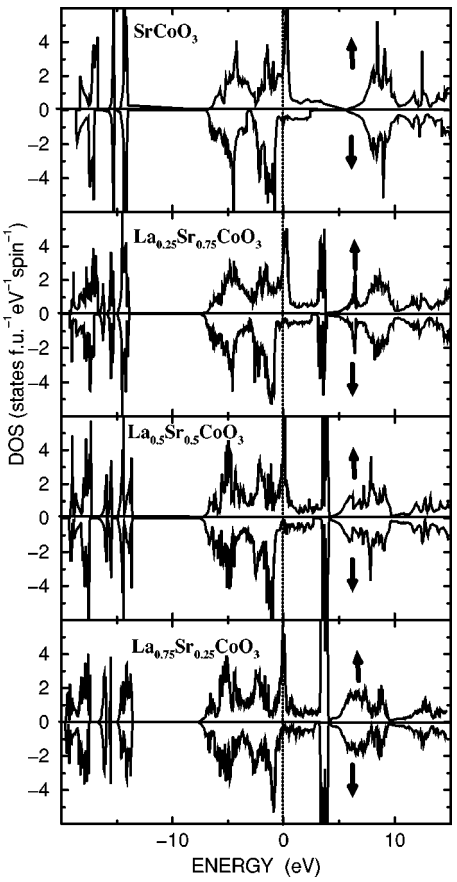

FIG. 4. Calculated total DOS for $La_{1-x}Sr_xCoO_3$ as obtained from supercell calculations. DOS refers to the rhombohedral structure for $x=0.25$ and 0.5 and to the cubic structure for $x=0.75$ and 1.

rhombohedral distortion is frequently not included in the attempt to explain the electronic structure of $LaCoO_3$. It is interesting to note that the overall shape of DOS for $LaCoO_3$ is quite different for the rhombohedral and cubic structures [see Figs. 2(a) and 2(b)]. In particular, the threefold degeneracy of the t_{2g} states and the twofold degeneracy of e_g states are partly lifted due to the reduction in symmetry.

In order to understand the changes which may occur in the electronic structure of $LaCoO_3$ we have considered hetrovalent Sr substitution and calculated DOS for $La_{1-x}Sr_xCoO_3$ as a function of x (Fig. 4) according to supercell approach with the experimental structural parameters as input. When we go from $La_{0.75}Sr_{0.25}CoO_3$ to $SrCoO_3$ according to this illustration, the bands get broader as a result of the increase in volume. Furthermore, due to the increased exchange splitting of the Co $3d$ bands (Fig. 4) on going from $x=0.25$ to 1, the magnetic moment increases almost linearly (Fig. 5). As Sr is divalent and La trivalent, removal of electrons from the CoO_3 sublattice is necessary to balance the charge deficiency introduced by the Sr substitution. Thus VB shows an upward shift towards the Fermi energy as a function of x (Fig. 4). This is consistent with experimental facts in the sense that the observed[60] ultraviolet photoemission spectra show that the nonbonding O $2p$ levels are shifted upwards with increasing Sr doping; ~ 0.2 eV for $x=0.2$ and ~ 0.5 eV for $x=0.5$. Moreover, VB photoemission spectra

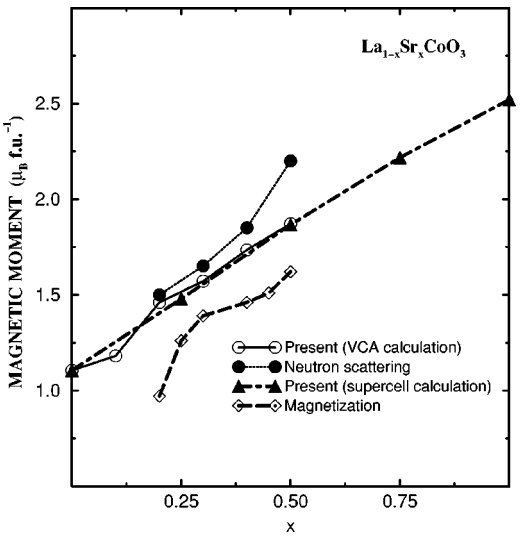

FIG. 5. Calculated magnetic moment for $La_{1-x}Sr_xCoO_3$ vs x as obtained by supercell and VCA calculations. Experimental magnetic moments are taken from neutron-scattering measurements (Ref. 9) at 4.2 K and magnetization measurements (Ref. 70) at 5 K.

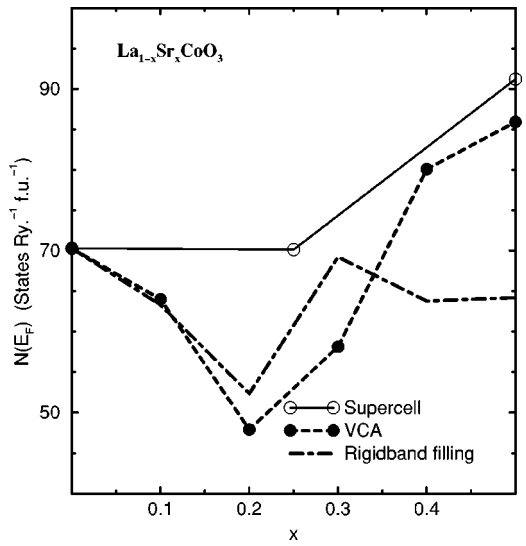

FIG. 6. DOS at E_F $[N(E_F)]$ for $La_{1-x}Sr_xCoO_3$ $(x=0-0.5)$ obtained from rigid-band-filling, supercell, and VCA calculations.

of $La_{1-x}Sr_xCoO_3$ show[32] that there is no rigid-band-like behavior in the VB spectrum as a result of the doping. Our calculated DOS curves also show significant changes introduced by the Sr substitution (Fig. 4). This indicates that hybridization and charge transfer effects play important roles in describing the electronic structure of $La_{1-x}Sr_xCoO_3$. As mentioned earlier, our calculations show that there is a sharp peak on the low-energy side of the Fermi level in $LaCoO_3$ and E_F falls on this peak for hole doping ($x<0.5$). This is consistent with the experimental findings in the sense that Hall coefficient measurements indicate the presence of a large Fermi surface in the conducting high-temperature phase and which is only little affected by moderate hole doping.[21]

To obtain a deeper insight into the role of the hole doping on changes of the electronic structure of $LaCoO_3$ near the Fermi energy, $N(E_F)$ values obtained from three different levels of approximation are shown as a function of x for $La_{1-x}Sr_xCoO_3$ in Fig. 6. In the rigid-band-filling calculations we have assumed that the shape of the DOS curve will not change by the Sr substitution. Hence, we have not taken into account the effects of changes in the hybridization effect and/or charge transfer. In the VCA calculations, we have included the experimentally observed changes in the structural parameters as a function of x. Hence, the hybridization effects are properly accounted for. However, the charge transfer effect is only taken into account in an averaged way. In the time-consuming supercell calculations we have dealt with all these effects properly. Assuming that the $N(E_F)$ values obtained from the supercell calculations are the most correct, we compare the $N(E_F)$ results obtained according to these three different procedures in Fig. 6. The calculated $N(E_F)$ for the range from $x=0$ to 0.25 obtained by the VCA and rigid-band-filling calculations are mutually comparable. However, the numerical values are smaller than those obtained by the supercell calculation. This indicates that it is important to account properly for the charge transfer between Sr and its neighbors and this is lacking in both VCA and rigid-band-filling calculations. For intermediate Sr concentrations $(0.4\leqslant x\leqslant 0.5)$ $N(E_F)$ obtained from the supercell and VCA calculations are more comparable indicating that the effect of charge transfer is less dominant. However, the large deviation in $N(E_F)$ between VCA and the rigid-band-filling calculation indicates that the hybridization is of importance in this composition range. Recent temperature dependent resistivity measurements[30,61] show that the semiconductor-to-metal transition takes place at 298 K around $x\approx 0.18$ in $La_{1-x}Sr_xCoO_3$. Our calculations do not confirm this feature, since our calculations suggest a metallic character throughout the substitution range (vide supra).

B. Structural stability and chemical bonding

The effective charges evaluated from the infrared reflectivity measurements of Tajima *et al.*[62] suggested that $La_{1-x}Sr_xCoO_3$ should have a high degree of covalent chemical bonding. Several other experimental studies[4,5,12,13,54,63] also point to the occurrence of substantial covalent interaction in $LaCoO_3$. In order to identify the bonding behavior we present the calculated valence charge density from -1 eV to E_F in the a plane which is equivalent to (110) plane in the cubic subcell [Fig. 7(b)]. According to Fig. 7(b) it is clear that there is a strong directional bonding between Co and O in $LaCoO_3$. The negligible charge density between La and CoO_3 as well as the very low electron population at the La site (much lower than for a neutral La atom) are clear indications of ionic bonding between La and CoO_3. Hence, $LaCoO_3$ may be viewed as composed of La^{3+} and $(CoO_3)^{3-}$. In order to understand the role of the chemical bonding on the rhombohedral distortion in $LaCoO_3$ we also show [Fig. 7(a)] the valence charge density from -1 eV to E_F in the (110) plane of a hypothetical cubic variant of $LaCoO_3$. The major difference between Figs. 7(a) and 7(b) is the strong covalent interaction between Co and O valence electrons in rhombohedral $LaCoO_3$ compared with the cubic variant for which the valence electrons near E_F are mainly in the nonbonding state. From this result it is clear that the rhombohedral distortion enhances the covalent interaction

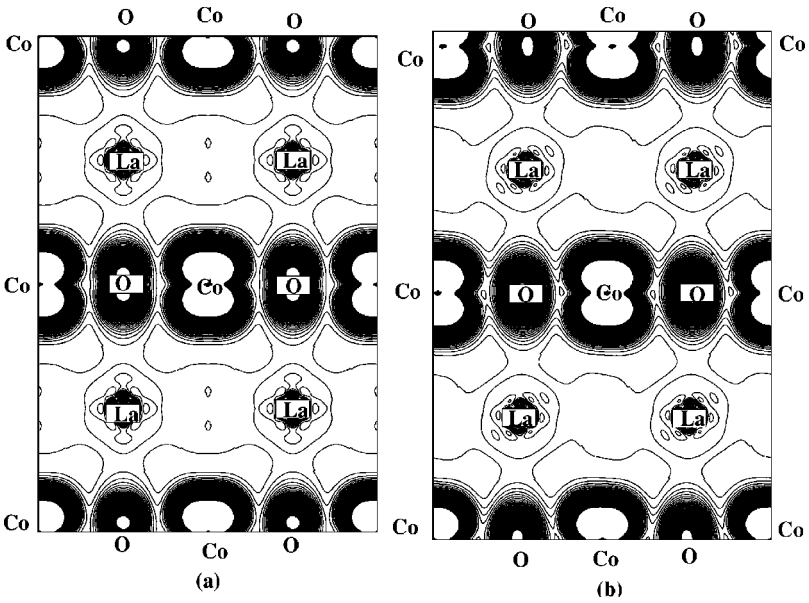

FIG. 7. Valence charge density contours for nonmagnetic $LaCoO_3$ in the (110) plane for (a) hypothetical cubic and (b) rhombohedral structures. The valence electrons in the range below E_F-1 eV to E_F are shown with the 90 contour line drawn between 0.001 and 0.08 electrons $(\text{a.u.})^{-3}$.

between Co and O and this gains the extra energy needed to stabilize the rhombohedral over the cubic phase. This also indicates that the appearance of the pseudogap according to our calculated DOS in the nonmagnetic rhombohedral phase of $LaCoO_3$ [Fig. 2(a)] is mainly originating from the covalent hybridization between Co and O.

A correlation exists between the location of E_F on the DOS curve and the structural stability of an intermetallic compound.[64] When we increase the Sr concentration the Co $3d$-like peak falls on the Fermi energy in the DOS curve and ferromagnetism arises. Also, owing to the coincidence of E_F and this peak, $N(E_F)$ increase with increasing Sr concentration (Fig. 6). For $x>0.5$, this peak moves away from the Fermi level as a result of the decreasing electron-to-atom ratio. As the stability of $La_{1-x}Sr_xCoO_3$ mainly originates from the covalent interaction between the Co $3d$ and O $2p$ electrons, lowering of the number of d electrons in the vicinity of the Fermi level at higher Sr concentration is expected to give rise to structural destabilization. This may be the reason for the experimentally reported[23,24] oxygen deficiency at high Sr concentrations in $La_{1-x}Sr_xCoO_3$.

In order to obtain a deeper insight into the chemical bonding behavior of $LaCoO_3$ we have given the angular momentum, site decomposed DOS in Fig. 3. Here the Co $3d$ and O $2p$ states are completely degenerate from the bottom of VB to E_F. This supports also the strong covalent interaction between Co and O. As mentioned above, the calculated charge density in the (110) plane of $LaCoO_3$ [Fig. 7(b)] also show evidence of the covalence between Co and O. The inferred covalence in $LaCoO_3$ is consistent with recent photoemission and x-ray absorption spectroscopy measurements.[32] In the upper panel of Fig. 3, the O $2s$ states are well separated from VB indicating that the O $2s$ electrons are not participating in the chemical bonding. In DOS for La, the peak structure ~ -15 eV arises from the pseudocore $5p$ states and are well separated from VB. Although the La $5p$ states are essentially localized from VB they show considerable dispersion (Fig. 3). In VB there is a negligible contribution coming from the La atoms (Fig. 3) indicating a nearly ionic situation for La. The sharp peak some 4 eV above E_F originates from La $4f$ states. In general the octahedral crystal field split the Co $3d$ states into t_{2g} and e_g bands. Owing to the rhombohedral distortion their degeneracy is lifted (Fig. 3).

The ionic radius of Sr^{2+} is larger than that of La^{3+}. Hence, when La^{3+} is replaced by Sr^{2+} there will act a negative chemical pressure on the CoO_3 units. This chemical pressure increases primarily the degree of tilting of the octahedra and hence the Co-O-Co bond angles as well as the overlap interaction increase which in turn results in a lengthening of the Co-O bonds in order to compensate for the local repulsion between overlapping charge densities. The lobes of the t_{2g} orbitals point between the oxygen ligands (π bond), whereas those of the e_g orbitals point directly at the ligands (σ bond). Hence, with Sr substitution the overlap with O $2p$ orbitals will be greater for e_g than t_{2g} orbitals. This may be the possible reason for why the e_g states shift to the unoccupied region of DOS by Sr substitution. Moreover, since Sr doping is equivalent to hole doping the number of electrons contained in VB decreases with increasing of Sr concentration. This leads to a systematic shift of E_F towards the lower energy region of DOS.

In order to understand the relative stability between various compositions of $La_{1-x}Sr_xCoO_3$, we have computed the total energy of $La_{1-x}Sr_xCoO_3$ in the cubic and rhombohedral structures for the ferromagnetic as well as the nonmagnetic cases (Fig. 8). Now we can analyze the possible electronic origin of the stabilization of the nonmagnetic rhombohedral structure in $LaCoO_3$. The total DOS of $LaCoO_3$ in the cubic, ferromagnetic and nonmagnetic phases is shown in Fig. 2(b). From this illustration it can be seen that the nonbonding t_{2g} electrons are piled up near E_F in the cubic, nonmagnetic case. This is an unfavorable condition for stability since the one-electron energy increases with increasing concentration of electrons closer to E_F. However, when we include spin polarization in the calculation the t_{2g} levels split in two parts. As this exchange splitting gives a gain in the total energy of the system, the ferromagnetic state becomes lower in energy than the nonmagnetic state (Fig. 8). So, if $LaCoO_3$ should occur as the hypothetical cubic phase, it would stabilize in the ferromagnetic state rather than the nonmagnetic state.

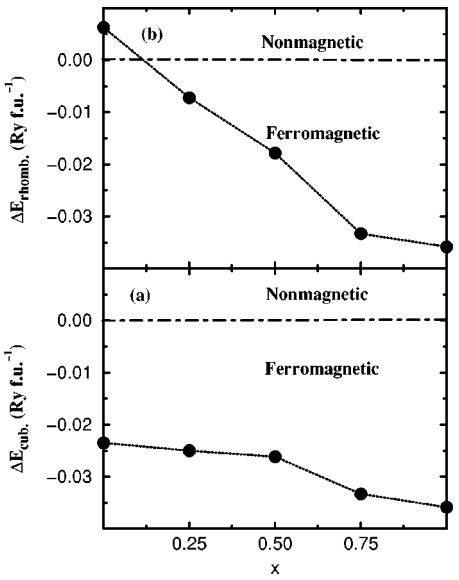

FIG. 8. Calculated total energy for (a) cubic and (b) rhombohedral phases of $La_{1-x}Sr_xCoO_3$ relative to their corresponding nonmagnetic states.

However, in the cubic, ferromagnetic phase E_F falls on a peak in the DOS curve as shown in Fig 2. Hence a Peierls-Jahn-Teller-like[65] instability arises and the system stabilizes in the lower symmetric rhombohedral structure. The Peierls-Jahn-Teller-like instability in the cubic phase accordingly arises from the orbital degeneracy of the e_g state. For the ferromagnetic and nonmagnetic phases of rhombohedral $LaCoO_3$, E_F falls on the nonbonding $3d$-like state in the ferromagnetic case and a pseudogap in the nonmagnetic case. Since the location of E_F on the pseudogap gives extra contribution to the structural stability,[64] $LaCoO_3$ stabilizes in the nonmagnetic, rhombohedral structure.

C. Origin of ferromagnetism

Replacing La with Sr introduces hole states above the Fermi level and reduces the electron per atom ratio in $LaCoO_3$. If we assume that the rigid-band-filling principle works in this case, the reduction in the electron per atom ratio is equivalent to shifting E_F towards the lower energy side of DOS. As there is a sharp peak in DOS at the lower energy part closer to E_F in nonmagnetic, rhombohedral $LaCoO_3$, Sr doping enhances $N(E_F)$. Hence the Stoner criterion $[N(E_F)I>1$; I being the Stoner parameter] for band ferromagnetism will be fulfilled and ferromagnetism will appear.

Goodenough[50] has pointed out that the magnetic moment of $1.5\mu_B$ in metallic $La_{0.5}Sr_{0.5}CoO_3$ can be rationalized with an intermediate-spin model having localized t_{2g}^5 configurations on each cobalt and an itinerant σ^* band containing 0.5 electrons per Co atom magnetized ferromagnetically. From magnetization measurements in low magnetic fields Itoh *et al.*[66] found that there exist spin-glass ($0<x\leqslant 0.18$) and cluster-glass ($0.18\leqslant x\leqslant 0.5$) regions in $La_{1-x}Sr_xCoO_3$ due to the random distribution of Sr and the competition between the ferromagnetic, double-exchange interaction between Co^{4+} and Co^{3+} and antiferromagnetic superexchange interactions between high-spin states such as $Co^{3+}-Co^{3+}$ and $Co^{4+}-Co^{4+}$. Recently Potze *et al.*[47] have studied x-ray absorption spectra of $SrCoO_3$ and concluded that the Co atoms in this material are in an intermediate spin ($t_{2g}^4e_g^1$, $S=1$) ground state. They also pointed out the possibility of an intermediate-spin state in slightly doped $LaCoO_3$. From magnetic susceptibility measurements on $La_{1-x}Sr_xCoO_3$ Ganguly *et al.*[61] found that Co^{3+} at low Sr substitution levels are in the IS-state configuration. Recently Yamaguchi *et al.*[67] inferred from temperature dependent infrared spectroscopy on $LaCoO_3$ that the splitting of phonon modes resulting from the spin-state transition and the local lattice distortion can be interpreted as related to the thermally excited IS-state spin transition in Co^{3+}. The substitution of Sr^{2+} for La^{3+} converts its nearest neighbor cobalts into a tetravalent low-spin (t_{2g}^5;LS), high-spin ($t_{2g}^3e_g^2$;HS), or intermediate-spin ($t_{2g}^4e_g^1$;IS) state. If we consider a purely ionic picture, the above spin configurations gives maximum $1\mu_B$, $5\mu_B$, and $3\mu_B$ per Co atom, respectively, in $SrCoO_3$. The strong O $2p$ to Co $3d$ hybridization reduces the exchange splitting of the t_{2g} bands, resulting in a small reduction in the magnetic moment of $La_{1-x}Sr_xCoO_3$ compared with the pure ionic configuration. Our calculated magnetic moment per Co atom in $SrCoO_3$ is $1.843\mu_B$ and this indicates that the IS configuration is more favorable than the LS and HS configurations at higher levels of Sr substitution.

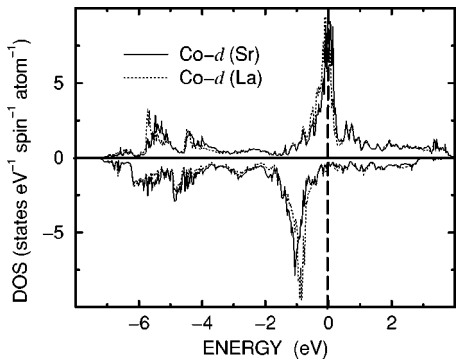

FIG. 9. Spin-projected d-electron DOS for a Co atom closer to La (dotted line) and closer to Sr (continuous line) in $La_{0.75}Sr_{0.25}CoO_3$ as obtained from the supercell calculations.

From their experimental results Raccah and Goodenough[19] concluded that the Co $3d$ electrons are in a localized state in the La-rich region of $La_{1-x}Sr_xCoO_3$, whereas they are collective and contribute to ferromagnetism in the Sr-rich region. Bhide *et al.*[22] measured the temperature dependence of Mössbauer spectra in the ferromagnetic region of iron doped $La_{1-x}Sr_xCoO_3$ ($0\leqslant x\leqslant 0.5$) and reported that ferromagnetic Co clusters in the Sr-rich region coexist with paramagnetic cobalt clusters in La-rich regions in a given sample. In order to understand the magnetic properties of the cobalt ions in regions close to the Sr and La clusters, spin polarized Co $3d$ DOS for Co atoms closer to La and Sr are presented in Fig. 9 for the $La_{0.75}Sr_{0.25}CoO_3$ case. These are obtained by the supercell approach based on experimental structural parameters as inputs. From this illustration it is clear that d states for the Co atoms in both configurations are itinerant and also that both are participating in the ferromagnetism. However, it is interesting to note that Co atoms closer to Sr are more spin polarized than those closer to La

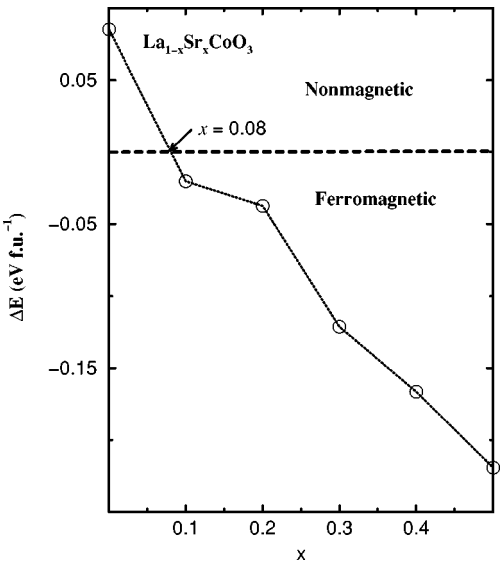

FIG. 10. Total energy of ferromagnetic $La_{1-x}Sr_xCoO_3$ vs x relative to the paramagnetic state obtained by VCA calculations.

(Co closer to La possesses a magnetic moment of $1.08\mu_B$ and those closer to Sr $1.40\mu_B$). This indicates that Co ions in neither of these configurations are in the Co^{3+} LS state in $La_{0.75}Sr_{0.25}CoO_3$. A small substitution of La by Sr in $LaCoO_3$ significantly changes the electronic structure of the Co ions throughout the lattice. Hence, the theoretical results rule out the possibility of stabilization of the Co $3d$ electrons in a localized state in the La-rich region of $La_{1-x}Sr_xCoO_3$. From ferromagnetic resonance measurements Bahadur *et al.*[68] found that the Lande factor takes a single value of 1.25 irrespective of the Sr^{2+} content in $La_{1-x}Sr_xCoO_3$. From this observation they proposed that the Co ions are in one single valence state in this material. Our calculated magnetic moments for Co close to La and Sr sites are not markedly different, indicating that the Co valence states do not differ much in $La_{1-x}Sr_xCoO_3$. As our calculated total magnetic moments (Fig. 5) are found to be in very good agreement with the low-temperature neutron-scattering measurements, we believe that the electrons contributing to magnetism in this material are of the itinerant-band, ferromagnetic character rather than of a localized nature.

D. Nonmagnetic to ferromagnetic transition

Magnetization measurements[24] indicate that the nonmagnetic-to-ferromagnetic transition appears in the composition range $0.05 \leqslant x \leqslant 0.15$. In order to simulate this transition we have calculated the energy difference between nonmagnetic and ferromagnetic states of $La_{1-x}Sr_xCoO_3$ as a function of x using VCA calculations. According to Fig. 10 the nonmagnetic-to-ferromagnetic transition takes place at $x=0.08$ which is in good agreement with experimental findings.[24] Also the stabilization of the ferromagnetic phase for $x>0.08$ is in agreement with the paramagnetic behavior observed in the susceptibility for $x>0.08$.[14] Furthermore our calculations show that the nonmagnetic state is 0.084 eV $f.u.^{-1}$ lower in energy than the ferromagnetic state in $LaCoO_3$. This is consistent with the experimental studies in the sense that the nonmagnetic state is the ground state for $LaCoO_3$. For the cubic and the rhombohedral structures, the differences in total energy between the ferromagnetic and nonmagnetic phases obtained by supercell calculations are shown in Figs. 8(a) and 8(b), respectively. Figure 8(b) places the nonmagnetic-to-ferromagnetic transition at $x=0.11$ which is in good agreement with the results obtained from VCA calculations. Hence, for $x>0.08-0.11$ the ferromagnetic phase is the energetically favored state as also confirmed experimentally[24].

The possibility of an intermediate-spin state with Fermi energy between localized t_{2g}^5 and t_{2g}^6 states has been postulated by Raccah and Goodenough[19] for $x=0.5$ (found to be a metallic ferromagnet). From temperature dependent electrical resistivity measurements Thornton *et al.*[12] explained the semiconductor-to-metal transition by stabilization of an intermediate-spin state associated with a smooth transition from localized e_g to itinerant σ^* electrons for the Co ions. Self-energy-correction-included HF calculations[53] show that the LS-to-IS transition takes place in $La_{1-x}Sr_xCoO_3$ at $x \approx 0.08$. It is interesting to note that the present calculations locate the nonmagnetic-to-ferromagnetic transition at the same composition (Fig. 10). This indicates that the nonmagnetic-to-ferromagnetic transition is associated with the spin-state transition in $La_{1-x}Sr_xCoO_3$. For the rhombohedral structure (note that our calculated total energy for the spin-polarized case is higher in energy than the nonmagnetic case) our calculations gave a magnetic moment of $1.1\mu_B$ $f.u.^{-1}$ for $LaCoO_3$. This indicates that although the nonmagnetic state represents the ground state in $LaCoO_3$, there exists a metastable solution with a magnetic moment of $1.1\mu_B$ $f.u.^{-1}$ for this phase. It is worth recalling that the pronounced field dependence of the magnetic susceptibility of $LaCoO_3$ ceases at ~ 100 K. Also, the removal of the dramatic field effect already at the substitution level $t=0.01$ in $LaCo_{1-t}Cr_tO_3$ supports the existence of closely spaced energy levels which are easily modified by small amounts of paramagnetic substituents.[69] The self-energy-corrected HF calculations[53] gave a magnetic moment of 2.12 and $3.49\mu_B$ $(Co\ atom)^{-1}$ for the IS and HS state of $LaCoO_3$, respectively. From LDA+U calculations, Korotin *et al.*[51] found 2.11 and $3.16\mu_B$ $(Co\ atom)^{-1}$, respectively. Our calculations thus suggest that the possible spin-state transition on temperature increase and/or hole doping is LS-to-IS rather than LS-to-HS. Furthermore, the small difference in the magnetic moment of the Co atoms closer to Sr and La in $La_{1-x}Sr_xCoO_3$ (Sec. IV C) appears to support this inference and consequently to the rejection of the LS-to-mixed-LS–HS-state transition proposed by Rodriguez and Goodenough.[70]

Our calculated magnetic moments for $La_{1-x}Sr_xCoO_3$ (VCA and supercell) are compared with the experimental low-temperature neutron-scattering measurements[9] in Fig. 5. Both experiment and theory show a trend of increased magnetic moment by hole doping. From saturation magnetization measurements on $La_{1-x}Sr_xCoO_3$ Jonker and van Santen[24] found that the magnetic moment increases with increasing x and takes $\sim 1.3\mu_B$ $(Co\ atom)^{-1}$ at $x=0.4$. For $x=0.5$ the experimentally observed magnetic moment is $2.2\pm 0.2\mu_B$ $(Co\ atom)^{-1}$. This shows that the agreement between experiment and theory is good. It is interesting to note that our

calculated magnetic moments obtained from the supercell and VCA calculations are mutually consistent (Fig. 5). This indicates the VCA approach is reliable to predict magnetic properties of transition metal oxides with hole doping. Furthermore, it should be noted that the magnetic moment obtained from low-temperature magnetization measurements[70] is always lower than those obtained from the theoretical calculations as well as from neutron-scattering measurements (Fig. 5). More recent saturation magnetization measurements[43] for $x=0.3$ at 4.2 K gave a moment of about $1.7\mu_B$ (Co atom)$^{-1}$. This indicates that the deviation between moments obtained from the magnetization measurements and the present theoretical study (Fig. 5) may be due to experimental errors. However, a discrepancy between experiment and theory above $x>0.5$ can be expected, because the oxygen deficiency is known to increase above $x\approx 0.5$, in particular if the samples are not prepared under a high oxygen pressure.[25,26]

The magnetic moments obtained for $x=0.2$ and 0.3 by VCA calculations are $1.46\mu_B$ and $1.57\mu_B$ (Co atom)$^{-1}$ and in good agreement with the experimental values[43] of 1.5 and $1.89\mu_B$ (Co atom)$^{-1}$ obtained at 10 K by neutron diffraction. From magnetization measurements[30] the estimated magnetic moment for $x=0.25$ at 10 K is $1.52\mu_B$ (Co atom)$^{-1}$ in good agreement with $1.47\mu_B$ (Co atom)$^{-1}$ obtained by the supercell calculations. It should be noted that the magnetic moment increases from $1.33\mu_B$ to $1.89\mu_B$ (Co atom)$^{-1}$ when the temperature is decreased from 300 to 10 K for $x=0.3$ [$1.18\mu_B$ to $1.5\mu_B$ (Co atom)$^{-1}$ for $x=0.2$].[43] The increasing trend in the magnetic moment as a function of Sr doping is mainly caused by the narrowing of the bands due to the increase in volume[43] (Fig. 4). The experimentally established[25] Curie temperature (T_C) increases monotonously with increasing x and reaches a maximum at $x=0.7$, whereafter it decreases linearly with increasing x in the range $0.8\leqslant x\leqslant 1.0$.[25] Our calculated magnetic moment as a function of x (Fig. 5) increases linearly with x indicating that the decrease in T_C for $x>0.7$ may be associated with the formation of oxygen vacancies.

In general one expects that the calculated magnetic moment for $SrCoO_3$ should be higher than that obtained experimentally. Since $La_{1-x}Sr_xCoO_3$ in practice will have oxygen deficiency at higher Sr substitution,[71] one must expect a lowering of the magnetic moment [the magnetic moment in $SrCoO_{3-\delta}$ vary from $\sim 0.85\mu_B$ to $1.6\mu_B$ (Co atom)$^{-1}$ depending on the oxygen stoichiometry[71]]. As our calculated magnetic moments are valid only for the ideal oxygen content, the calculated value for $SrCoO_3$ [$2.52\mu_B$ (Co atom)$^{-1}$] will be larger than the experimental values [$1.8\mu_B$ (Co atom)$^{-1}$ according to linear extrapolation of Fig. 3 in Ref. 71].

V. SUMMARY

We have made detailed investigation of the role of hole doping on electronic structure and magnetic properties of $LaCoO_3$ using supercell approach as well as VCA calculations. We have inferred the following.

(1) Our calculations show that the nonmagnetic state is the ground state for $LaCoO_3$ in agreement with experimental observations.

(2) We have identified strong covalent interactions between Co and O within the CoO_6 octahedra and ionic bonding between La and these building units in $LaCoO_3$.

(3) The density functional calculations with gradient corrections fails to predict the narrow bandgap semiconducting behavior. Instead it predicts a pseudogap at E_F.

(4) The rhombohedral distortion in the nonmagnetic cubic phase is originating from Peierls-Jahn-Teller-type instability.

(5) The nonmagnetic to ferromagnetic transition in $La_{1-x}Sr_xCoO_3$ takes place around $x=0.08$ in the VCA calculations and $x=0.11$ in the supercell calculations. These values are in good agreement with the experimentally reported values (for $x=0.05$ to 0.15).

(6) The calculated magnetic moments are found to be in good agreement with the experimental values, suggesting that the magnetic properties of $La_{1-x}Sr_xCoO_3$ can be explained through itinerant-band ferromagnetism.

(7) Present results indicate that the formal Co^{4+} in $La_{1-x}Sr_xCoO_3$ are closer to the IS configuration rather than to LS or HS configuration.

(8) The calculations suggest that the possible spin state transition induced in $LaCoO_3$ by hole doping is from LS to IS rather than from LS to HS or from LS to a mixed LS and HS state.

ACKNOWLEDGMENTS

P.R. is grateful for financial support from the Research Council of Norway. P.K. acknowledges financial support from the SKB AB, the Swedish Nuclear Fuel and Waste Management Company. P.R. is also grateful to Professor B. Johansson and Dr. O. Eriksson for their encouragements, Dr. J. M. Wills for generously making his program available for the present studies, and to Dr. Lars Nordström and Dr. H.W. Brinks for the useful discussions.

*Electronic address: ravindran.ponniah@kjemi.uio.no

[1] J.G. Bednorz and K.A. Müller, Z. Phys. B: **64**, 189 (1986).
[2] R. von Helmolt, J. Wecker, B. Holzapfel, L. Shultz, and K. Samwer, Phys. Rev. Lett. **71**, 2331 (1993).
[3] J. Zaanen, G.A. Sawatzky, and J.W. Allen, Phys. Rev. Lett. **55**, 418 (1985).
[4] M. Abbate, J.C. Fuggle, A. Fujimori, L.H. Tjeng, C.T. Chen, R. Potze, G.A. Sawatzky, H. Eisaki, and S. Uchida, Phys. Rev. B **47**, 16 124 (1993).
[5] A. Chainani, M. Mathew, and D.D. Sharma, Phys. Rev. B **46**, 9976 (1992).
[6] R.R. Heikes, R.C. Miller, and R. Mazelsky, Physica (Amsterdam) **30**, 1600 (1964).
[7] V.G. Bhide, D.S. Rajoria, G. Rama Rao, and C.N.R. Rao, Phys. Rev. B **6**, 1021 (1972).
[8] K. Asai, P. Gehring, H. Chou, and G. Shirane, Phys. Rev. B **40**, 10 982 (1989).
[9] M. Itoh and J. Natori, J. Phys. Soc. Jpn. **64**, 970 (1995).

[10] S.R. Barman and D.D. Sarma, Phys. Rev. B **49**, 13 979 (1994).
[11] P.M. Raccah and J.B. Goodenough, Phys. Rev. **155**, 932 (1967).
[12] G. Thornton, B.C. Tofield, and D.E. Williams, Solid State Commun. **44**, 1213 (1982).
[13] G. Thornton, F.C. Morrison, S. Partington, B.C. Tofield, and D.E. Williams, J. Phys. C **21**, 2871 (1988).
[14] K. Asai, O. Yokokura, N. Nishimori, H. Chou, J.M. Tranquada, G. Shirane, S. Higuchi, Y. Okajima, and K. Kohn, Phys. Rev. B **50**, 3025 (1994).
[15] C.S. Naiman, R. Gilmore, B. DiBartolo, A. Linz, and R. Santoro, J. Appl. Phys. **36**, 1044 (1965).
[16] S. Yamaguchi, Y. Okimoto, H. Taniguchi, and Y. Tokura, Phys. Rev. B **53**, R2926 (1996).
[17] G.H. Jonker, J. Appl. Phys. **37**, 1424 (1966).
[18] N. Menyuk, P.M. Raccah, and K. Dwight, Phys. Rev. **166**, 510 (1967).
[19] P.M. Raccah and J.B. Goodeneough, J. Appl. Phys. **39**, 1209 (1968).
[20] W.C. Koehler and E.O. Wollan, J. Phys. Chem. Solids **2**, 100 (1957).
[21] Y. Tokura, Y. Okimoto, S. Yamaguchi, H. Taniguchi, T. Kimura, and H. Takagi, Phys. Rev. B **58**, R1699 (1998).
[22] V.G. Bhide, D.S. Rajoria, V.G. Jadhao, G. Rama Rao, and C.N.R. Rao, Phys. Rev. B **12**, 2832 (1975).
[23] A. Mineshige, M. Inaba, T. Yao, Z. Ogumi, K.K. Kuchi, and M. Kawase, J. Solid State Chem. **121**, 423 (1996).
[24] G.H. Jonker and J.H. van Santen, Physica (Amsterdam) **19**, 120 (1953).
[25] H. Taguchi, M. Shimada, and M. Koizumi, Mater. Res. Bull. **13**, 1225 (1978); J. Solid State Chem. **33**, 169 (1980); **29**, 221 (1979).
[26] H. Taguchi, M. Shimada, and M. Koizumi, Mater. Res. Bull. **15**, 165 (1980).
[27] P.W. Anderson, Phys. Rev. **79**, 350 (1950); **79**, 705 (1950).
[28] C. Zener, Phys. Rev. **82**, 403 (1951).
[29] J.B. Goodenough, J. Phys. Chem. Solids **6**, 287 (1958).
[30] V. Golovanov, L. Mihaly, and A.R. Moodenbaugh, Phys. Rev. B **53**, 8207 (1996).
[31] P.W. Anderson, Phys. Rev. Lett. **64**, 1839 (1990); **67**, 2092 (1991).
[32] T. Saitoh, T. Mizokawa, A. Fujimori, M. Abbate, Y. Takeda, and M. Takano, Phys. Rev. B **56**, 1290 (1997).
[33] F.R. van Buren, G.H.J. Broers, A.J. Bouman, and C. Boesveld, J. Electroanal. Chem. Interfacial Electrochem. **88**, 353 (1978).
[34] A.G.C. Kobussen, F.R. van Buren, and G.H.J. Broers, J. Electrochem. Soc. **91**, 211 (1978).
[35] C.S. Tedmon, Jr., H.S. Spacil, and S.P. Mitoff, J. Electrochem. Soc. **116**, 1170 (1969).
[36] Y. Kaga, Y. Ohno, K. Tsukamoto, F. Uchiyama, M.J. Lain, and T. Nakajima, Solid State Ionics **40/41**, 1000 (1990).
[37] Y. Teraoka, H. Zhang, S. Furukawa, and N. Yamazoe, Chem. Lett. **48**, 1743 (1985).
[38] T. Nakamura, M. Misono, T. Uchijima, and Y. Yoneda, Nippon Kagaku Kaishi, **1980**, 1679.
[39] R.J.H. Voorhoeve, J.P. Remeika, and L.E. Trimble, *The Catalytic Chemistry of Nitrogen Oxides* (Plenum Press, New York, 1975), p. 215.
[40] S. Yamaguchi, H. Taniguch, H. Takagi, T. Arima, and Y. Tokura, J. Phys. Soc. Jpn. **64**, 1885 (1995).
[41] G. Briceno, X.-D. Xiang, H. Chang, X. Sun, and P.G. Schultz, Science **270**, 273 (1995).
[42] C. Michel, J.M. Moreau, and W.J. James, Acta Crystallogr., Sect. B: Struct. Crystallogr. Cryst. Chem. **27**, 501 (1971).
[43] V.G. Sathe, A.V. Pimpale, V. Siruguri, and S.K. Paranjpe, J. Phys.: Condens. Matter **8**, 3889 (1996).
[44] J.M.Wills (unpublished); J.M. Wills and B.R. Cooper, Phys. Rev. B **36**, 3809 (1987); D.L. Price and B.R. Cooper, *ibid.* **39**, 4945 (1989).
[45] O.K. Andersen, Phys. Rev. B **12**, 3060 (1975).
[46] J.P. Perdew, in *Electronic Structure of Solids*, edited by P. Ziesche and H. Eschrig (Akademie Verlag, Berlin, 1991), p. 11; J.P. Perdew, K. Burke, and Y. Wang, Phys. Rev. B **54**, 16 533 (1996); M.R. Pederson and D.J. Singh, *ibid.* **46**, 6671 (1992).
[47] R.H. Potze, G.A. Sawatzky, and M. Abbate, Phys. Rev. B **51**, 11 501 (1995).
[48] J.B. Goodenough, *Progress in Solid State Chemistry*, edited by H. Reiss (Pergamon, London, 1971), Vol. 5, p. 145; *Solid State Chemistry*, edited by C.N.R. Rao (Dekker, New York, 1974).
[49] T. Arima, Y. Tokura, and J.B. Torrance, Phys. Rev. B **48**, 17 006 (1993).
[50] J.B. Goodenough, Mater. Res. Bull. **6**, 967 (1971).
[51] M.A. Korotin, S.Y. Ezhov, I.V. Solovyev, V.I. Anisimov, D.I. Khomskii, and G.A. Sawatzky, Phys. Rev. B **54**, 5309 (1996).
[52] I. Solovyev, N. Hamada, and K. Terakura, Phys. Rev. B **54**, 5368 (1996).
[53] M. Takahashi and J. Igarashi, Phys. Rev. B **55**, 13 557 (1997).
[54] M. Abbate, R. Potze, G.A. Sawatzky, and A. Fujimori, Phys. Rev. B **49**, 7210 (1994).
[55] N. Hamada, H. Sawada, and K. Terakura, in *Spectroscopy of Mott Insulators and Correlated Metals*, edited by A. Fujimori and Y. Tokura, Springer Series in Solid-State Sciences (Springer Verlag, Berlin, 1995), p. 95.
[56] D.D. Sarma, N. Shanthi, S.R. Barman, N. Hamada, H. Sawada, and K. Terakura, Phys. Rev. Lett. **75**, 1126 (1995).
[57] F. Munakata, H. Takahashi, Y. Akimune, Y. Shichi, M. Tanimura, Y. Inoue, R. Itti, and Y. Koyama, Phys. Rev. B **56**, 979 (1997).
[58] T. Saitoh, A.E. Bocquet, T. Mizokawa, and A. Fujimori, Phys. Rev. B **52**, 7934 (1995).
[59] S. Masuda, M. Aoki, Y. Harada, H. Hirohashi, Y. Watanabe, Y. Sakisaki, and H. Kato, Phys. Rev. Lett. **71**, 4214 (1993).
[60] J.P. Kemp, D.J. Beal, and P.A. Cox, J. Solid State Chem. **86**, 50 (1990).
[61] P. Ganguly, P.S. Anil Kumar, P.N. Santhosh, and I.S. Mulla, J. Phys.: Condens. Matter **6**, 533 (1994).
[62] S. Tajima, A. Masaki, S. Uchida, T. Matsuura, K. Fueki, and S. Sugai, J. Phys. C **20**, 3469 (1987).
[63] G. Thornton, A.F. Orchard, and C.N.R. Rao, J. Phys. C **9**, 1991 (1976).
[64] J.-H. Xu, T. Oguchi, and A.J. Freeman, Phys. Rev. B **35**, 6940 (1987); J.-H. Xu and A.J. Freeman, *ibid.* **40**, 11 927 (1989); **41**, 12 553 (1990); J. Mater. Res. **6**, 1188 (1991); P. Ravindran, G. Subramoniam, and R. Asokamani, Phys. Rev. B **53**, 1129 (1996).
[65] P. Söderlind, O. Eriksson, B. Johansson, J.M. Wills, and A.M. Boring, Nature (London) **374**, 524 (1995); R. Peierls, *More Surprises in Theoretical Physics* (Princeton University Press, Princeton, 1991).
[66] M. Itoh, I. Natori, S. Kubota, and K. Motoya, J. Phys. Soc. Jpn. **63**, 1486 (1994).

[67] S. Yamaguchi, Y. Okimoto, and Y. Tokura, Phys. Rev. B **55**, R8666 (1997).
[68] D. Bahadur, S. Kollali, C.N.R. Rao, M.J. Patni, and C.M. Srivastava, J. Phys. Chem. Solids **58**, 981 (1979).
[69] B. G. Tilset, H. Fjellvåg, A. Kjekshus, and B.C. Hauback, Acta Chem. Scand. **52**, 733 (1998).
[70] M.A.S. Rodriguez and J.B. Goodenough, J. Solid State Chem. **116**, 224 (1995).
[71] H. Tacuchi, M. Shimada, and M. Koizumi, J. Solid State Chem. **22**, 221 (1979).